

See discussions, stats, and author profiles for this publication at: <https://www.researchgate.net/publication/282706046>

Role of Casting Solvent on Nanoparticle Dispersion in Polymer Nanocomposites

ARTICLE *in* MACROMOLECULES · JULY 2014

Impact Factor: 5.8

READS

25

3 AUTHORS, INCLUDING:



Dan Zhao

Columbia University

6 PUBLICATIONS 11 CITATIONS

[SEE PROFILE](#)



Sanat K. Kumar

Columbia University

288 PUBLICATIONS 7,365 CITATIONS

[SEE PROFILE](#)

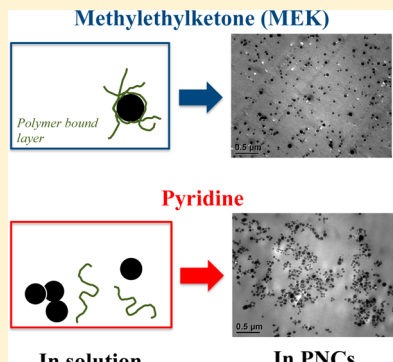
Role of Casting Solvent on Nanoparticle Dispersion in Polymer Nanocomposites

Nicolas Jouault, Dan Zhao, and Sanat K. Kumar*

Department of Chemical Engineering, Columbia University, 500 W. 120th St., New York, New York 10027, United States

Supporting Information

ABSTRACT: We investigate the influence of casting solvent on the final spatial dispersion of nanoparticles (NPs) in polymer nanocomposites (PNCs). We prepared nanocomposites of bare silica NPs and poly(2-vinylpyridine) (P2VP) by casting from two different solvents—methyl ethyl ketone (MEK) and pyridine—which are theta/good solvents, respectively, for both the polymer and the NPs. In MEK, we show that P2VP strongly adsorbs onto the silica surface to create a temporally stable bound polymer layer. The resulting “hairy” particles are sterically stabilized against agglomeration, and thus good NP dispersion in PNCs is always achieved, independent of P2VP molecular weight, concentration, or NP loading. On the contrary, in pyridine, P2VP does not adsorb on the silica NPs. The phase behavior in this case is thus governed by a subtle balance among electrostatic repulsion, polymer-induced depletion attraction, and the kinetic slowdown of diffusion-limited NP aggregation. While there is little remnant solvent in the dry PNC, and since these dispersion states are hardly altered on annealing, these results serve to emphasize the crucial role played by the casting solvent in the spatial dispersion state of NPs in a polymer matrix.



I. INTRODUCTION

Polymer nanocomposites (PNCs), i.e., NPs dispersed in a polymer matrix, have attracted interest over the past few decades since they can have enhanced macroscopic properties relative to the pure polymer.¹ It is now commonly accepted that the dispersion of the NPs in the polymer matrix controls the final properties of the PNCs² and that this dispersion state can be tuned by varying the energetic interaction between the NPs and the polymer or by controlling entropic factors. Thus, it is believed that NPs will be well-dispersed in a polymer if their energetic interactions are favorable, while immiscibility should otherwise result. Entropic control over polymer–NP miscibility can be most readily realized by grafting polymer chains onto the NP surface. This leads to complex phase and self-assembly behavior depending on the grafting density and the grafted/matrix chain length ratio.³ Another scenario was presented by Mackay et al.,⁴ who established a miscibility diagram for bare NPs with a variety of systems (dendritic polyethylene, fullerenes (C_{60}), or cross-linked polystyrene (PS) dispersed in linear PS prepared by the rapid precipitation method). Since their results were apparently independent of the chemistries of the NPs and the polymers, these workers proposed the following general strategy for the dispersion of NPs in a polymer matrix. When the NP radius, R_{NP} , is larger than the radius of gyration R_g of the polymer, the PNC displays immiscibility, i.e., NP aggregation. However, when R_{NP} is smaller than R_g good NP dispersion is predicted. In addition to these “equilibrium” factors underpinning NP dispersion, other mechanisms can also be employed to control NP morphologies,

e.g., external (shear flow,⁵ elongation) or internal (e.g., block copolymers)⁶ factors.

While each of these approaches is individually interesting, they do not take into account the processing parameters used for creating PNCs. Our basic premise, which is echoed by multiple anecdotal pieces of evidence, is that processing strongly affects the initial NP dispersion state. Subsequent annealing does not alter this state significantly (especially in cases involving high molecular weight, M_w , matrices), and hence the initial processing step is critical to the NP dispersion state and the properties obtained from this class of hybrid materials. Multiple processing techniques have been used to prepare PNCs:⁷ melt mixing, extrusion, compression molding, rapid precipitation, or solvent casting. We focus here on solvent casting, in particular properly enunciating the sketchily documented role of the choice of solvent and its evaporation rate on NP dispersion. For instance, for 14 nm diameter bare silica/PS PNCs, different solvents, e.g., methyl ethyl ketone (MEK),⁸ tetrahydrofuran (THF),⁸ or dimethylacetamide (DMAc),⁹ have been found to give different dispersion states when the solvent is evaporated slowly—from large spherical aggregates (in THF) to small fractal aggregates (in DMAc). Even if the compatibility between NP and polymer is improved (by changing the nature of the polymer), the same progression of solvent driven dispersion state is observed.^{9b} However, if the solvent is allowed to evaporate quickly, NP dispersion is always

Received: March 26, 2014

Revised: May 21, 2014

Published: July 15, 2014



improved.¹⁰ Another example was reported by Janes et al.,¹¹ who showed that exposing PNCs to different solvent vapors can alter the NP structures from uniform dispersion to agglomeration. In the same vein, Meth and co-workers¹² showed that the aggregation of charged silica NPs in low M_w PS or poly (methyl methacrylate) (PMMA) matrices occurred during the drying process when around half of the solvent (DMF in that case) had evaporated. The aggregation comes from a collapse of the charged double layer (due to changes in dissociation equilibrium of $-OH$ groups at the silica surface). Additionally, these authors observed good NP dispersion due to the decrease of NP diffusion when the polymer M_w becomes high (i.e., when the viscosity of the solution increases). Zukoski's group¹³ studied silica/polyethylene glycol (PEG)/ethanol (or water) systems in various regimes of polymer concentration (from dilute to melt). By combining scattering techniques (light scattering, SANS, and SAXS) and theory, they correlated the NPs miscibility with the existence of a dense PEG layer (around 1 nm thick) adsorbed at the silica surface. They thus concluded that the polymer/silica attraction strength is the key parameter in determining NP dispersion. Similarly, we showed that a poly(2-vinyl pyridine) (P2VP) bound layer is formed around silica NPs in MEK solution, with a thickness comparable to the R_g of the chains.¹⁴ Good NP dispersion is obtained due to the steric stabilization afforded by these bound layers, in apparently good agreement with the Zukoski et al. work.

While there have therefore been many works on the role of casting solvent on NP dispersion, a comprehensive understanding of the physics of these situations does not exist. Here, we critically investigate the role of the casting solvent on the silica dispersion in PNCs, in the particular case where the NPs and the polymer segments have strongly favorable attractions to each other.¹⁵ We prepared PNCs composed of spherical, as-received silica NPs and P2VP (with a M_w ranging from 2.4K to 940K), from two different solvents (MEK or pyridine) and studied this preparation procedure through a combination of dynamic and static light scattering (DLS and SLS) on NP/polymer solutions and TEM on dry PNCs. We show that the final dispersion can be tuned from a well-dispersed state (due to polymer adsorption or through kinetic effects) to an aggregated regime induced by depletion attraction and weakening of electrostatic repulsion simply by changing the solvent used. These results point emphatically to the role of preparation conditions, i.e., primarily the solvent-induced effective interactions between the NPs and the polymers, on the final NP dispersion in a PNC.

II. MATERIALS AND METHODS

II.1. Materials. All materials were used as received. Methyl ethyl ketone (MEK or 2-butanone, HPLC grade >99.7%) and pyridine (ACS agent, >99.0%) were ordered from Sigma-Aldrich. Seven different poly(2-vinylpyridine)s (P2VP) with molecular weights M_w ($M_w = 2400$, $M_w/M_n = 1.20$; $M_w = 14\,700$, $M_w/M_n = 1.05$; $M_w = 54\,000$, $M_w/M_n = 1.08$; $M_w = 105\,000$, $M_w/M_n = 1.08$; $M_w = 302\,000$, $M_w/M_n = 1.09$; $M_w = 554\,000$, $M_w/M_n = 1.11$; $M_w = 940\,000$, $M_w/M_n = 1.10$) were obtained from Polymer Source. The colloidal silica NPs (MEK-ST-L, 40–50 nm diameter, and MEK-ST, 10–15 nm diameter) were donated by Nissan Chemical Industries and are partially treated NPs but with silanol groups still available at the surface.¹⁶ Antioxidant Irganox 1010, donated by BASF Switzerland, was used to avoid thermal degradation during annealing at 150 °C.

II.2. Static and Dynamic Light Scattering (SLS and DLS).¹⁷ The light scattering measurements used a BI-200SM (Brookhaven

Instruments) equipped with diode-pumped solid state (DPSS) laser operating at $\lambda = 532$ nm and a BI-9000 AT digital correlator. We also performed DLS measurements using a Zetasizer NanoZS (Malvern Instruments) equipped with a 633 nm HeNe laser, operating at a scattering angle of 173° (backscattering setup). For the measurements the solutions were prepared as follows. First, a pure NP solution is diluted to a concentration of 0.13 wt %. Then, P2VP is added to this solution and stirred for 1 day with a vortex mixer to ensure polymer dissolution. Measurements were done in a glass cuvette, and samples were filtered with 0.45 μm PTFE filters. The details of DLS and SLS are presented in the Supporting Information. Briefly, the hydrodynamic radius R_h is obtained from the Stokes-Einstein relation (eq 8 in Supporting Information) and depends on the temperature, the viscosity of the medium (see below), and the diffusion coefficient D . At one given scattering angle, the apparent diffusion coefficient D_{app} is measured and its extrapolation to $q = 0$ gives the mutual diffusion coefficient D_0 . We compared the R_h calculated from the D_0 (using different angles from 40° to 140°) with the one from the D_{app} obtained at one given angle (173° using Zetasizer Nano ZS instrument) and found similar results for solutions characterized by a single relaxation mechanism, i.e., one population in size, and dominated by a diffusive process (i.e., characteristic time $\tau \approx q^{-2}$) (see Figure S0 in Supporting Information). However, for solutions characterized by two relaxation mechanisms (as at high P2VP concentrations, see below) the extrapolation is no longer valid, and the CONTIN analysis giving an intensity size distribution, valid in all cases, was used (already defined in the instruments software). As a consequence, to compare all the samples, we chose to present our data using the intensity size distribution from the CONTIN analysis and defined the hydrodynamic diameter D_h as the maximum position.

II.3. Viscosity of Bulk Solution. Proper interpretation of the DLS measurements requires knowledge of the viscosity of the bulk solution (at least for high polymer concentration). The solution viscosity was measured using a Viscopro 2000 (Cambridge viscosity) at 25 °C. The data for one case (302K P2VP) are shown in Figure S1 of the Supporting Information; note that adding silica NPs at low concentrations (0.13 wt %) did not modify the viscosity. The data can be fitted by using the Huggins expression:¹⁸

$$\eta = \eta_0(1 + [\eta]C + k'[\eta]^2C^2) \quad (1)$$

where η_0 is the solvent viscosity (0.4 and 0.88 cP at 25 °C for MEK and pyridine, respectively). $[\eta]$ is the literature value of the intrinsic viscosity ($[\eta]_{P2VP/MEK}$ (mL/g) = $0.093 \times M_w$ (g/mol)^{0.48} and $[\eta]_{P2VP/pyridine}$ (mL/g) = $0.00445 \times M_w$ (g/mol)^{0.78} for MEK and pyridine, respectively),¹⁹ and k' is the Huggins constant and determined as $k' = 0$ for MEK and $k' = 0.387$ for pyridine systems. Then, from the intrinsic viscosity one can calculate the overlap concentration $C^* = 1/[\eta]$ for P2VP in both MEK and pyridine (see Table S1 in Supporting Information).

II.4. ζ-Potential and Conductivity Measurements. The ζ -potential measurements were performed on a Zetasizer Nano ZS (Malvern Instruments) at 25 °C. The ζ -potential, known as the electrostatic potential at the hydrodynamic slipping plane close to a surface, is determined from the measurement of the electrophoretic mobility μ_e using the Henry function with the Smoluchowski approximation.²⁰ The electrical conductivity of the solution can also be found from the same instrument.

II.5. Nanocomposite Preparation. Solvent-casting was used to prepare nanocomposite films by co-casting P2VP and silica composite solutions in either MEK or pyridine. First, the as-received Nissan silica suspensions were diluted with MEK or pyridine in the volume ratio of 3:7. The resulting silica dispersion was sonicated for 2 min. Immediately after that, the actual concentration of silica particles in this dilute dispersion was precisely determined by dropping 100 μ L of solution into each of four open alumina vessels, evaporating until there is no change in weight, and then weighing the residual nonvolatile materials. The average value of these four measurements was taken as the true concentration, which was approximately 100 mg/mL. In parallel, P2VP and antioxidant Irganox (0.2 wt % relative to polymer)

solutions in MEK or pyridine were prepared in 12 mL Teflon-capped glass vials. This was then vortex-shaken for at least 2 h (depending on molecular weight of P2VP) to guarantee complete polymer dissolution. Appropriate amounts of the diluted silica dispersion (being sonicated again for 2 min right before mixing with polymer solution) were added to the polymer/Irganox solution, resulting in P2VP/silica formulations with a known weight ratio. Most of the composite solutions obtained were vortex-shaken for 24 h and then probe ultrasonicated for 3 min using a Ultrasonic Processor (model GEX-750) operated at 24% of maximum amplitude with a pulse mode of 2 s sonication following by 1 s rest. For the kinetic studies, varying periods of time, ranging from 1 h to several months, were used to vortex-mix certain composite solutions before probe sonication. Finally, the composite solutions were directly poured into 60 mm diameter Petri dishes and evaporated for 5 days in a fume hood before being examined by transmission electronic microscopy. To characterize NP organization in real space, a strip of bulk PNC (several hundred micrometers in thickness) was embedded in epoxy resin, cured at 80 °C for 8 h, and then cut into slices with thickness around 60 nm using ultramicrotomy. These slices were floated on a Formvar-coated copper TEM grid from deionized water and visualized in a Jeol JEM-100 CX electron microscope. Unless noted otherwise, the TEM images were taken for as-cast films.

III. RESULTS AND DISCUSSION

III.1. Behavior in Solution. III.1.1. Bare NP in Solvents. Figure 1 shows the scattering intensity, or the Rayleigh ratio $R(q)$, obtained by SLS measurements for dilute 50 nm silica NPs in (a) MEK (0.02 wt %) and (b) pyridine (0.057 wt %). Because the silica concentration is low, the interaction between NPs can be neglected (i.e., no correlation peak in the scattering

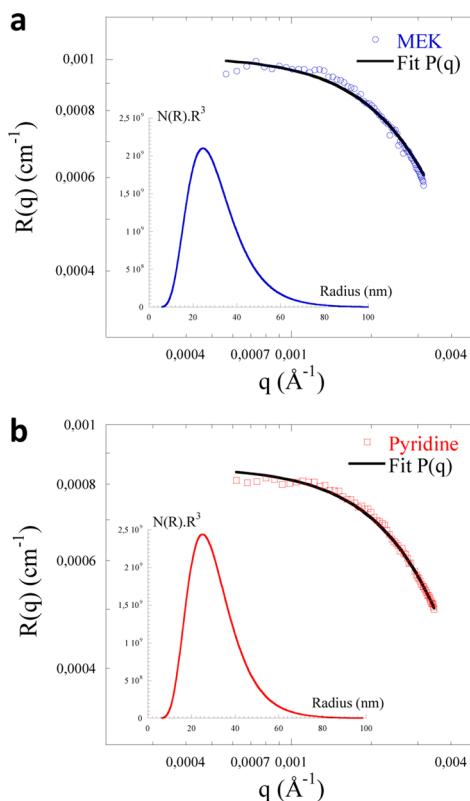


Figure 1. Rayleigh ratio $R(q)$ obtained by SLS measurements of dilute 50 nm bare silica in (a) MEK (0.02 wt %) and (b) pyridine (0.057 wt %). The black continuous lines correspond to the fits using a polydisperse spherical form factor $P(q)$ with a log-normal distribution. The insets show the corresponding size distributions.

curves), and thus $R(q)$ is only proportional to the silica form factor $P(q)$.

The curves are well-fit with a polydisperse sphere form factor with a log-normal distribution with two parameters: the radius R_0 and the polydispersity σ . The size distributions are shown in the insets to Figure 1, and Table 1 presents the results. Both R_0

Table 1. Structural Parameters of Silica NPs in MEK and Pyridine

parameters	MEK	pyridine
dielectric constant ϵ_r	17.5	12.5
R_0^a (nm)	28.8	28.8
σ^a	0.40	0.37
$\langle R \rangle^b$ (nm)	24.6	25.0
R_h (DLS)/ R_v (DLS) (nm)	44.5/27	42/27
R_g (nm) ^c	36	32.5
R_g/R_h	0.81	0.77
ζ^d (mV)	-40	-33

^aFrom fitting $P(q)$ to dilute solutions. ^bMaximum in log-normal size distribution. ^cFrom SLS at silica concentration of 0.057 wt % for pyridine and 0.02 wt % for MEK. ^dSilica concentration: 0.13 wt %.

and σ are similar in the two solvents ($R_0 = 28.8$ nm and $\sigma = 0.4$), indicating that the transfer into pyridine does not affect the stability of the NP dispersion. The Guinier regime at low q gives a radius of gyration R_g of 36 and 32.5 nm for MEK and pyridine, respectively. We also performed DLS measurements leading to a hydrodynamic radius R_h (from the intensity size distribution) of 44.5 and 42 nm for MEK and pyridine, respectively (i.e., $R_g/R_h = 0.81$ and 0.77, commonly observed for spherical objects). Note that the conversion from intensity to volume distribution leads to a radius R_v of 27 nm (close to R_0 from SLS fitting and the size provided by Nissan Chemical). The discrepancy between R_h and R_v is due to the polydispersity of the native NPs.

The ζ -potentials measured for one silica concentration (0.13 wt %) are -40 and -33 mV for MEK and pyridine, respectively, indicating that the NPs are stabilized by negative charges coming from the dissociation of the surface silanol groups. The charge dissociation mechanism is due to the electron donor behavior of both MEK and pyridine. The difference in ζ -potentials between MEK and pyridine can be explained by the lower dielectric constant ϵ_r of pyridine leading to a lower dissociation at the silanol groups (Table 1). Adding salt, which screens the electrostatic repulsion between NPs, also proved the presence of charges (see Figure S2 in Supporting Information).

At high silica concentrations (up to 2 wt %), a correlation peak or a structure factor, $S(q)$, (coming from the interaction between NPs) appears for both systems (Figure 2). Since $R(q) \propto cP(q)S(q)$, we need models for both pieces. As before, $P(q)$ is modeled by a polydisperse sphere form factor with a log-normal size distribution. We now need a way of estimating the structure factor. Since the NPs are negatively charged, $S(q)$ can be calculated following the rescaled mean spherical approximation (RMSA) model first developed by Hayter and Penfold for macroions.²² In this model we fix the hard sphere radius $\langle R \rangle$ (determined at low concentrations), the volume fraction Φ , the temperature T , and the dielectric constant ϵ . The unknown parameters are the ion concentration [ion] and the effective charge number Z. With a knowledge of the ion concentration one can calculate the Debye length κ^{-1}

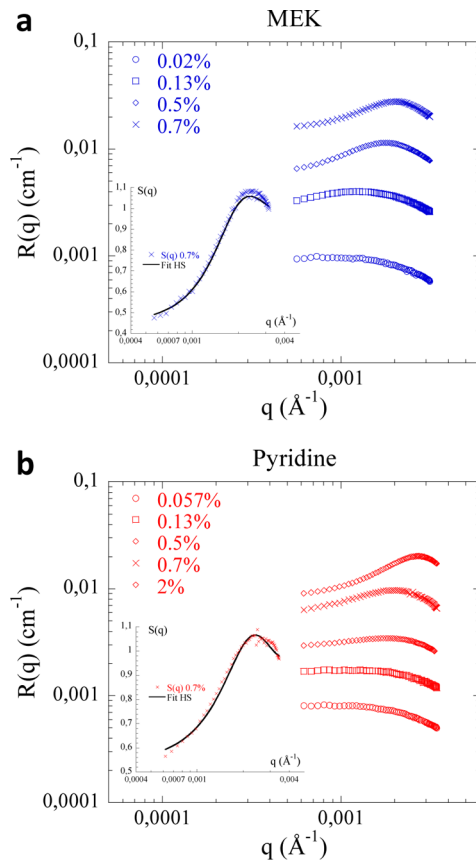


Figure 2. Rayleigh ratio $R(q)$ obtained by SLS measurements for (a) MEK and (b) pyridine at different silica concentrations. The curves have been shifted for clarity. In insets are shown the structure factor $S(q)$ at 0.7 wt % fitted with a hard sphere (HS) model.²¹

corresponding to the thickness of the electrical double layer around the silica NPs. In MEK at 0.13 wt % the best fit gives $Z = 85$ and $[\text{ion}] = 1.9 \times 10^{-9} \text{ M}$ (assuming monovalent ions) giving a Debye length $\kappa^{-1} = 4664 \text{ nm}$. Since the interparticle distance (ID) is estimated to be 575 nm, this questions the validity of the RMSA model in this context. To overcome this difficulty, the electrostatic repulsion can also be mapped into an effective hard sphere (HS) interaction.²³ The “effective” object is a silica core surrounded by a charged corona with a thickness δ_{HS} .¹² The fitting parameters of the HS model²¹ are an effective hard sphere radius R_{effHS} and an effective volume fraction Φ_{effHS} . Tables S1 and S2 present the results from this analysis (see Supporting Information). Assuming that $\delta_{\text{HS}} \approx \kappa^{-1}$, one can calculate the corresponding monovalent ion concentration. For 0.13 wt % we obtained 1.9×10^{-6} and $5.3 \times 10^{-6} \text{ M}$ for MEK and pyridine, respectively, which are significantly larger than the ones obtained by the RMSA model.

Another strategy to obtain the ion concentration is to measure the conductivity σ of the solution, which can be expressed as²⁴

$$\sigma = \frac{e^2 n_{\text{ion}}}{6\pi\eta R_{\text{ion}}} \quad (2)$$

where n_{ion} is the number density of ions, η is the solution viscosity, and R_{ion} is the hydrodynamic radius of the ion (here $R_{\text{ion}} = 1 \text{ nm}$). Then, using the value of n_{ion} , one can determine $\kappa = (4\pi\lambda_B n_{\text{ion}})^{1/2}$. At 0.13 wt % one obtains $[\text{ion}] = 5.38 \times 10^{-5} \text{ M}$ in MEK and $[\text{ion}] = 6.66 \times 10^{-5} \text{ M}$ in pyridine, close to

values recently obtained in similar systems.¹² The determination of the ion concentration allows us to calculate the total interaction potential V_{tot} between a pair of NPs²⁵ as expressed by

$$V_{\text{tot}} = V_{\text{VdW}} + V_{\text{electro}} \quad (3)$$

For bare silica, V_{tot} is the sum of the attractive van der Waals interaction V_{VdW} and the repulsive electrostatic repulsion V_{electro} . The electrostatic potential V_{electro} is

$$\frac{V_{\text{electro}}(h)}{kT} = \left(\frac{e\zeta}{kT} \right)^2 \frac{R_{\text{NP}}^2}{\lambda_B} \frac{\exp(-\kappa h)}{h + 2R_{\text{NP}}} \quad (4)$$

where $\lambda_B = e^2/(4\pi\epsilon_0 kT)^{1/2}$ is the Bjerrum length for monovalent ions, e the elementary charge, ζ the zeta-potential, κ^{-1} the Debye length, and h the interparticle separation distance. The core–core VdW attraction between a pair of NPs in solution is

$$V_{\text{vdW}}(h) = -\frac{R_{\text{NP}}}{12h} [(\sqrt{A_{\text{solvent}}} - \sqrt{A_{\text{SiO}_2}})^2] \quad (5)$$

The Hamaker constant A_H is defined as²⁵

$$A_H = \frac{3}{4} k_B T \left(\frac{\epsilon_i - \epsilon_{\text{vac}}}{\epsilon_i + \epsilon_{\text{vac}}} \right)^2 + \frac{3hv_e}{16\sqrt{2}} \frac{(n_i^2 - n_{\text{vac}}^2)^2}{(n_i^2 + n_{\text{vac}}^2)^3/2} \quad (6)$$

where k_B is the Boltzmann constant, T is the temperature (= 298 K), ϵ is the dielectric constant, h is Planck's constant, $v_e = 3.2 \times 10^{15} \text{ s}^{-1}$ is the main electronic absorption frequency, and n is the refractive index.

Figure 3 shows the results of this calculation. While the inter-NP potential has a long-range repulsion due to the relatively

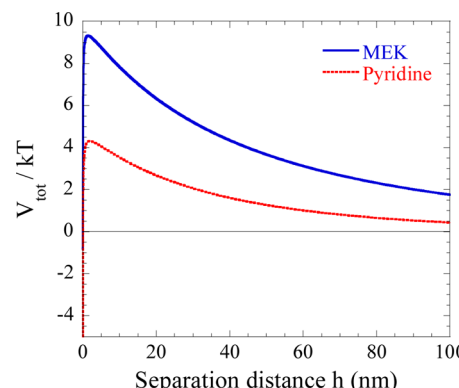


Figure 3. Total pair potential interaction V_{tot} for bare NPs in MEK (blue continuous line) and pyridine (red dashed line) at 0.13 wt %. The ion concentration is determined from HS fits.

low ion concentration in the solutions, the net repulsive barrier is significantly higher in MEK than in pyridine ($9kT$ vs $4kT$). Finally, we stress that the uncertainty in the determination of ion concentration is due to our lack of information about the commercial NPs (unknown surface chemistry and unknown ion nature and concentration).

III.1.2. Silica/P2VP/Solvent Ternary Systems. We now examine the effect of adding various amounts of P2VP to the silica solutions. We kept the silica concentration unchanged at 0.13 wt % and measured the hydrodynamic diameters D_h by DLS. Figure 4 shows the intensity size distribution (obtained using CONTIN analysis on our data) for two P2VP M_w s, 302K and 14.7K, respectively, in MEK and pyridine. We defined R as

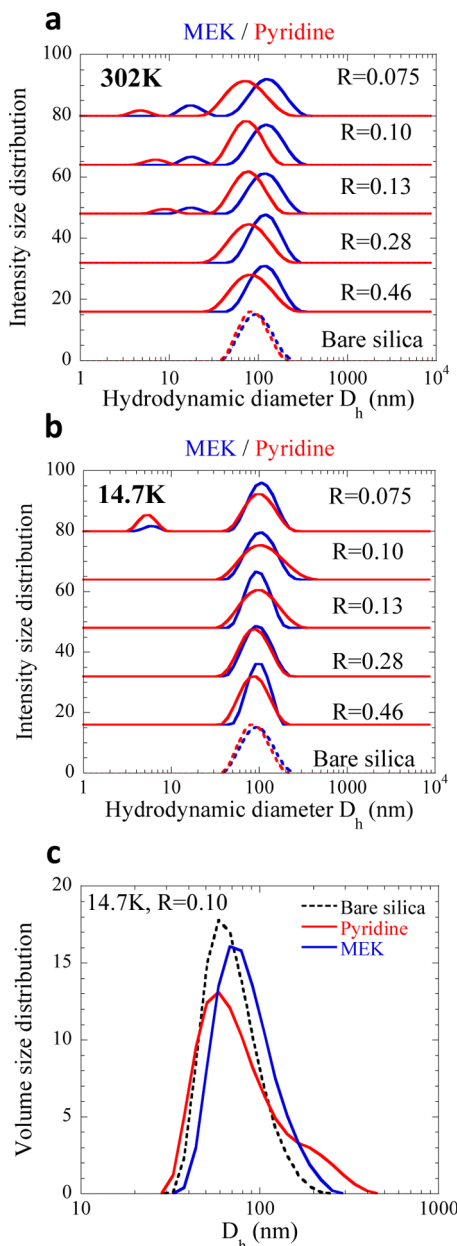


Figure 4. Intensity size distribution obtained by DLS measurement for (a) 302K and (b) 14.7K P2VP/silica in MEK (blue) and pyridine (red) for different ratio R . R is defined as the silica to polymer concentration ratio. The silica concentration is fixed at 0.13 wt %. (c) Volume size distribution for bare silica (black dashed line) and for 14.7K P2VP/silica in MEK (blue) and pyridine (red).

the silica to polymer concentration ratio: the decrease of R reflects the increase of P2VP concentration.

We first examine the case of 302K P2VP (Figure 4a). In MEK, at high R ($R = 0.46$, i.e., low P2VP concentration), the maximum of the size distribution shifts to larger D_h compared to bare silica (dashed lines) and then remains constant for lower R values. In pyridine, the position of the maximum remains similar to the bare silica for all R . Figure 5 displays D_h (maximum position in the size distribution from Figure 4a,b) as a function of P2VP concentration.

D_h increases abruptly on the addition of P2VP in MEK while it is not affected in pyridine. The increase in size in MEK is comparable to $2R_g$ of the chains (upper marker line in Figure

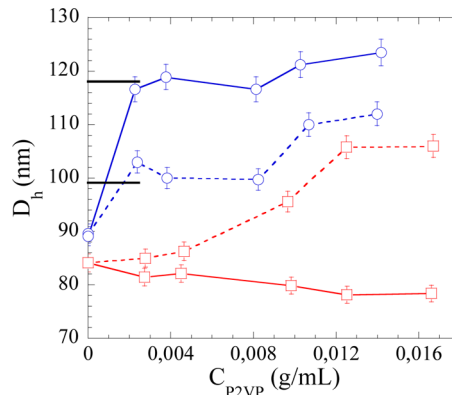


Figure 5. Hydrodynamic diameter D_h as a function of P2VP concentration in MEK (blue circles) and pyridine (red squares) for 14.7K (dashed lines) and 302K (continuous lines) P2VP.

5), suggesting that P2VP adsorbs to the silica surface in MEK to form a bound layer.¹⁴ Note that, at low R (i.e., high P2VP concentration), a second population is observed—this is related to free polymer chains with a D_h around 17 nm in MEK and 10 nm in pyridine ($R = 0.13$).

For the 14.7K P2VP in MEK, an increase in size is observed with a value close to $2R_g$. Note that, for high P2VP concentration, D_h increases due to possible bridging (this will be discussed later). However, in the pyridine case, an increase occurs with a broadening of the distribution (as clearly observed for $R = 0.13$ and 0.10 in Figure 4b). In Figure 4c the intensity size distribution has been converted into a volume size distribution for the specific case of $R = 0.10$, revealing the existence of two size populations for pyridine: one comparable to the bare silica and another one around 200 nm corresponding here to silica aggregates. In MEK only one population is observed with a size larger than the bare silica. Thus, in pyridine, the broadening and apparent increase of D_h in intensity size distribution are due to a coexistence of bare NPs and aggregates.

These results in solution suggest that (i) P2VP adsorbs on the silica surface in MEK, forming a bound layer of thickness R_g , thus preventing silica aggregation.²⁶ Note that in MEK the bound layer formed in solution is still present in the dry PNCs.¹⁴ (ii) P2VP does not adsorb in pyridine, and the silica forms aggregates for low M_w (14.7K) while it remains stable for higher M_w (302K). Presumably, the pyridine acts as a P2VP displacer preventing polymer adsorption:²⁷ the bare NPs then agglomerate due to depletion flocculation.

III.2. Effect of Solvent on Ultimate Silica Dispersion in Dried PNCs. Figure 6 presents TEM images for as-cast dry films of 50 nm diameter silica/14.7K P2VP PNCs prepared by solvent casting using MEK (a) or pyridine (b). Good dispersion of silica NPs is achieved when MEK is used as a solvent, independent of composition or the P2VP M_w . Previous work has shown that these results are insensitive to NP size as well.¹⁴ We believe that, following Figure 3, the silica NPs are stabilized against agglomeration by the presence of a bound P2VP layer that forms in MEK. Note that for larger P2VP concentrations (>0.012 g/mL), the NPs start to aggregate due to possible NP bridging;²⁸ the corresponding PNCs have heterogeneous NP dispersion (see Supporting Information Figure S3). One way to avoid this agglomeration phenomenon is to add a small amount of pyridine,²⁹ which presumably reduces the solvent-mediated

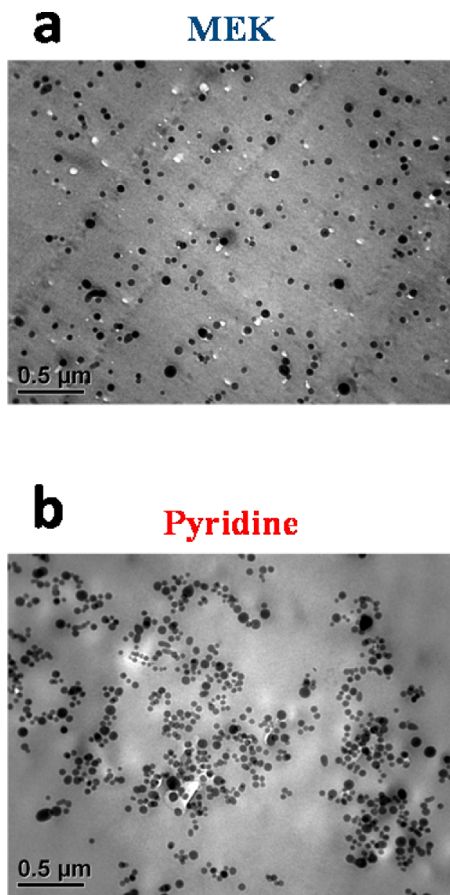


Figure 6. TEM of as-cast 10 wt % 50 nm bare silica NPs in a 14.7K P2VP matrix prepared by the solvent casting method using (a) MEK or (b) pyridine as a solvent.

attraction between the polymer and NPs^{28b} and thus reduces bridging and therefore flocculation.

In contrast to the good dispersion obtained with MEK, NPs form large aggregates when pyridine is used as the solvent (Figure 6b). (This effect is confirmed by the calculation of the correlation function $C(r)$ for both images in Figure 6; see Figure S4 in Supporting Information.) We also explored the influence of the P2VP M_w on the final NP dispersion (Figure 7). For low (14.7K, 54K) and high (554K, 940K) M_w s, NP aggregation is observed. Surprisingly, for intermediate M_w , better dispersion results. Again, the $C(r)$ confirms these observations (see Figure S5). We emphasize here that there is no bound polymer layer on the silica NPs in pyridine solution, which persists in the solid state as confirmed by the $C(r)$ in Figure 8 from the TEM image shown in Figure 7c (for details of this calculation we refer to our previous study¹⁴).

Clearly, the $C(r)$ can be almost reproduced by a pure hard sphere potential, but note that there is a slight deviation in the initial slope. Since we only input the size of the NPs (and the size distribution), and since the initial slope is determined by these quantities alone in the absence of NP aggregation, this deviation implies the existence of small aggregates in pyridine-cast samples. Thus, while we conclude that there is no polymer bound layer in the dry PNC, some other mechanism should be promoting dispersion for the intermediate M_w s. In the following, we argue that the good dispersion in 105K P2VP is due to a balance between electrostatic repulsion, polymer-induced depletion attraction, and kinetic slowdown of NP

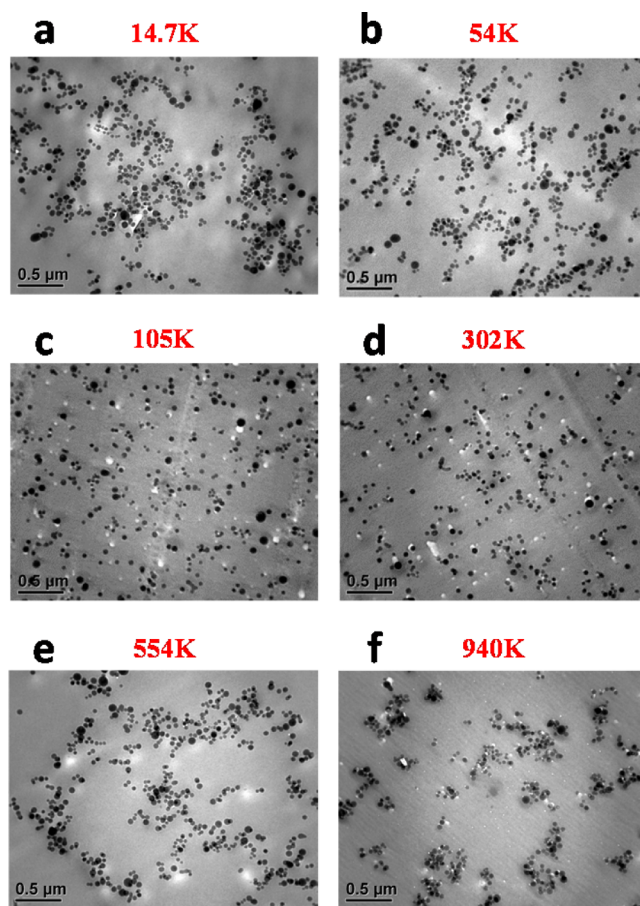


Figure 7. TEM images of as-cast 50 nm silica/P2VP PNCs prepared using pyridine for different P2VP M_w s: (a) 14.7K, (b) 54K, (c) 105K, (d) 302K, (e) 554K, and (f) 940K.

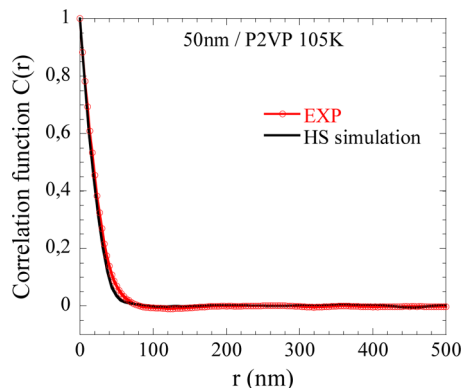


Figure 8. Correlation function $C(r)$ from TEM image of 50 nm/105K P2VP PNCs prepared using pyridine. The continuous black line is the simulation assuming a hard sphere (HS) potential between NPs.

diffusion, depending on the P2VP concentration in solution and the time of mixing before the solvent is evaporated. However, our results to this point suggest that in most cases the solvent determines the effective interaction between silica and polymer and thus controls the final dispersion.

III.3. Concentration- and Time-Dependent Evolution of NP Dispersion in Pyridine. We now focus on the unusual M_w dependence observed in the pyridine case. The phase behavior of silica/P2VP/pyridine ternary systems was monitored by SLS after 1 day of mixing. Figure 9a shows the

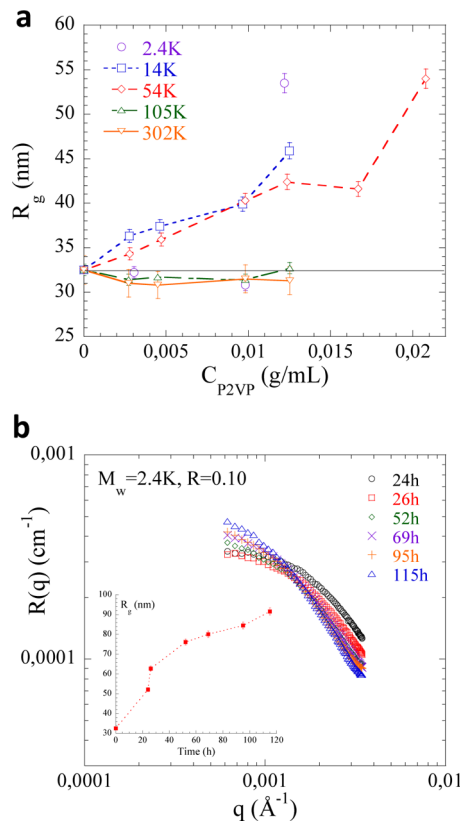


Figure 9. (a) Evolution of the R_g as a function of P2VP concentration for different P2VP M_w s in pyridine. The continuous line represents the R_g of bare silica (i.e., 32.5 nm). The silica concentration is fixed to 0.13 wt %. (b) Rayleigh ratio $R(q)$ of 2.4K P2VP/50 nm/pyridine for different time of mixing. Inset: evolution of R_g as a function of time.

evolution of R_g as a function of P2VP concentration for different M_w s. Because P2VP does not adsorb on the NP in pyridine, an increase in R_g must be associated with NP aggregation. Clearly, the lower the P2VP M_w , the faster the increase of R_g . For 105K and 302K no increase in R_g is observed in this range of concentration. We also follow the evolution of R_g with time for $M_w = 2.4\text{K}$ for $R = 0.10$ (i.e., $C = 0.012 \text{ g/mL}$, Figure 9b). We clearly observe an increase in R_g with time, indicating that the NP dispersion is not stable.

We also study the effect of solvent evaporation on NP dispersion in the dilute regime. For that, SLS measurements have been performed on silica/P2VP/pyridine solutions in which we fix $R = 0.13$ and vary the silica and P2VP concentrations simultaneously, simulating the drying process in its early stages. Figures 10a and 10c show the scattering intensity $R(q)$ normalized by the silica weight fractions from SLS for 14.7K (a) and 302K (b) P2VP systems.

For 14.7K one can see an increase of $R(q)$ at low q for 0.5 and 0.7 wt %, indicating the formation of aggregates in solution, while it remains flat for 302K. To explain this behavior, we estimated the total NP pair interaction potential V_{tot} in the presence of nonadsorbing polymer at different concentrations. Figures 10b and 10d show the results. The nonadsorbing polymer adds a depletion attraction between the NPs, $V_{\text{depletion}}$, to eq 3 as defined first by Asakura and Oosawa³⁰ and then extended by Vrij³¹ and de Gennes³² to semidilute solutions:

$$\frac{V_{\text{depletion}}(h)}{kT} = -\frac{2}{3}\pi n_p \Delta^3 \left(1 - \frac{h}{2\Delta}\right)^2 \left(2 + \frac{3R_{\text{NP}}}{\Delta} + \frac{h}{2\Delta}\right) \quad \text{in dilute regime} \quad (7)$$

$$\frac{V_{\text{depletion}}(h)}{kT} = \frac{R_{\text{NP}}}{\xi^3} \left(\xi - \frac{h}{2}\right)^2 \quad \text{in semidilute regime} \quad (8)$$

Here n_p is the polymer concentration, h is the separation distance, and Δ is the depletion layer thickness defined by³³

$$\frac{\Delta}{R_g} = \frac{1}{q} \left[\left(1 + \frac{6q}{\sqrt{\pi}} + 3q^2\right)^{1/3} - 1 \right] \quad \text{with } q = R_g/R_{\text{NP}} \quad (9)$$

Note here that above C^* the depletion range scales as ζ , i.e., decreases as C_{P2VP} increases, but its amplitude is larger. At the same time we observed a drastic change in conductivity before and after adding P2VP, suggesting that P2VP carries ions into the solutions. (We have tried to “clean up” these solutions through repeated washings but find that these “ions” do not get removed. We thus do not know the origins of these ions.) As a consequence, the electrostatic potential is largely modified with the disappearance of the long-range repulsion for the low M_w . This makes the NPs dispersion unstable, and it becomes easier to form aggregates once a collision between two NPs occurs.

While this logic explains the low- M_w behavior, it does not explain our TEM observations which showed that NPs apparently do not aggregate for 105K and 302K. We attribute this to a combination of two factors. First, as Figure 10d shows, a secondary weak maximum appears as the concentration of the solution is increased. This fact, coupled to an increase of bulk viscosity, leads to a slowdown of NP diffusion, i.e., a decrease of NP diffusion coefficient D_0 ¹² (Figure 11). At high concentration $D_{0-302\text{K}}$ is 10 times smaller than in 14.7K, indicating a significant slowdown of NP diffusion. These arguments are bolstered by the fact that the measurements in Figure 10 have been done 1 day after mixing the polymer with the NPs solution.

Figure 12 shows TEM images of 105K, 302K, and 554K P2VP PNCs prepared after mixing different times (0, 1, and 5 days) from pyridine. As the NP dispersion becomes unstable with time, aggregation occurs for all M_w s after 5 days (and 1 day for 554K), pointing to the fact that NP dispersion in these cases is a subtle balance between charge-induced NP–NP repulsion, polymer-induced attraction, and kinetic effects.

These results suggest that one can achieve good dispersion if (i) the P2VP concentration is low in the initial solution and (ii) the time between the preparation and the evaporation is short enough to “freeze” the NPs in good dispersion. This effect is NP size dependent. Figure 13 shows TEM images for 14 nm/105K P2VP prepared using MEK (a) and pyridine (b). As expected, the NPs are well dispersed when using MEK due to P2VP adsorption. When using pyridine, aggregation is observed (in contrary to 50 nm silica size, see upper left TEM image in Figure 13) because the electrostatic barrier is not high enough to prevent the depletion-induced NP flocculation. After long thermal annealing (10 days at 150 °C), the NP dispersion remains relatively unchanged in PNCs cast from MEK. However, for the pyridine-cast films, the NPs dispersion is improved upon thermal annealing, but with small direct NP–NP aggregates, which are hard to anneal away in an experimentally realistic time scale. Therefore, we conclude

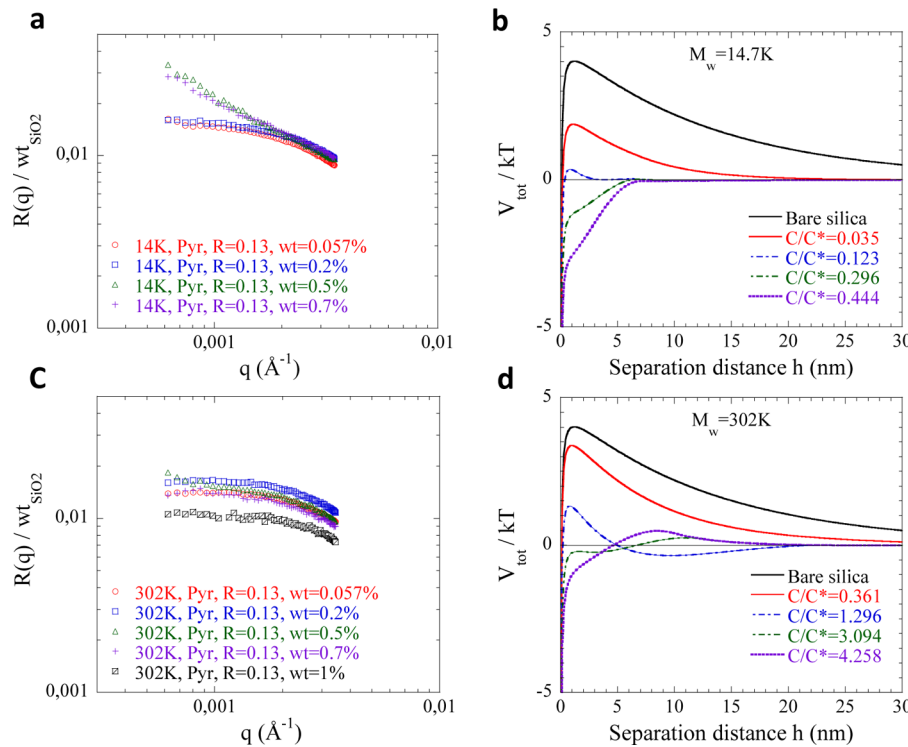


Figure 10. Rayleigh ratio $R(q)$ from SLS normalized by the silica weight fractions wt_{SiO_2} for 14.7K (a) and 302K (c) P2VP systems at different silica concentration (from 0.057 to 1 wt %). For this experiment the silica to polymer concentrations ratio is fixed at $R = 0.13$. (b) and (d) show the corresponding total pair interaction potential V_{tot}/kT for 14.7K (b) and 302K (d).

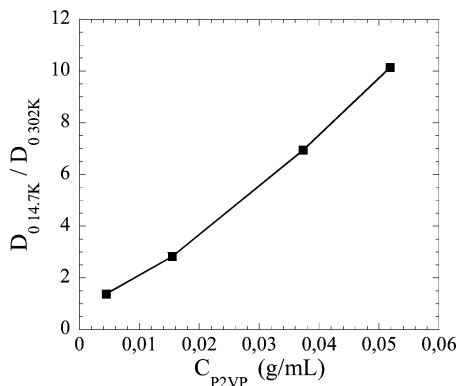


Figure 11. Evolution of $D_{0-14.7K}/D_{0-302K}$ as a function of P2VP concentration (assuming NPs remain individually dispersed).

that the practically final NP dispersion state is controlled by solution state from which they are formed.

Let us finally propose a criterion to generalize our findings to other systems. The hydrogen bonding energy between 2VP and silanol groups at the NP surface is estimated to be $\approx 10kT$ (without solvent). However, the solvent may affect the strength of this interaction and modify the NP/polymer stability. Polymer chains may preferentially adsorb on the NP surface in a poorer solvent to reduce contacts with solvent molecules.³⁴ Schweizer and co-workers²⁸ establish a phase diagram based on the interaction strength ϵ between polymer and NP. At low and high ϵ phase separation is expected due to polymer-induced depletion attraction or polymer bridging respectively, while moderate ϵ induces steric stabilization behavior. As a consequence, a solvent with moderate affinity for the polymer will induce polymer adsorption and finally individual NP

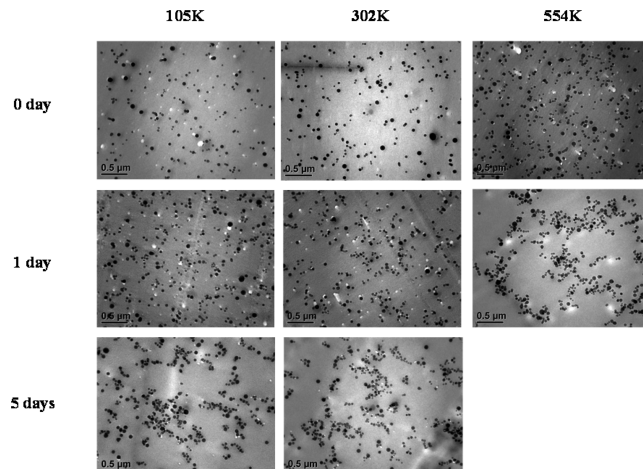


Figure 12. TEM images of 50 nm/P2VP filled with 10 wt % silica for 105K, 302K, and 554K after different times of mixing: 0, 1, and 5 days.

dispersion in PNCs. Quantitatively, one possible criteria for the solvent selection might be the Hansen solubility parameter δ . Polymer/solvent miscibility occurs if the δ of the two materials are similar. Here the δ values are 21.3, 19.3, and 21.7 MPa^{1/2} for P2VP, MEK, and pyridine, respectively. As δ_{P2VP} and δ_{pyridine} are similar, we hypothesize that pyridine is a better solvent for P2VP reducing ϵ . Such analysis should be strengthened with further investigations on different systems.

IV. CONCLUSION

The stability of NP dispersions in a polymer matrix depends on different forces such as short-range van der Waals (VDW) attraction, long-range electrostatic repulsion (due to the

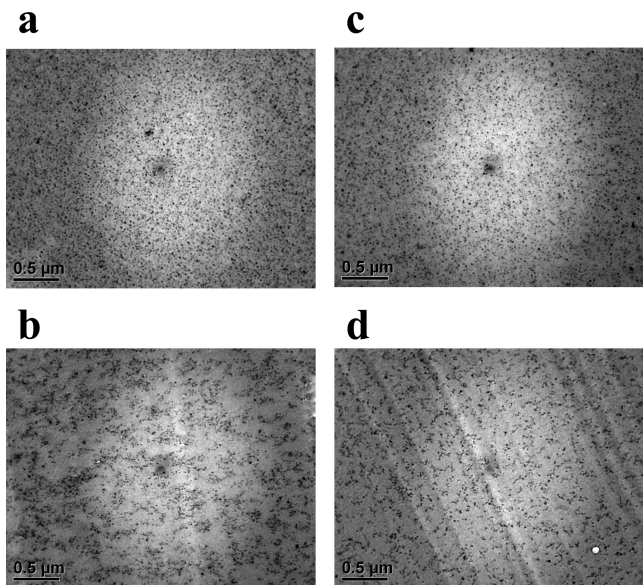


Figure 13. TEM of 10 wt % 14 nm bare silica NPs in a 105K P2VP matrix prepared by the solvent casting method using (a) MEK or (b) pyridine as a solvent before annealing. The solutions were cast 1 day after mixing. TEM images of the same samples after annealing at 150 °C during 10 days using (c) MEK or (d) pyridine.

existence of charges at the silica surface), steric repulsion (if polymer adsorbs), and polymer-induced depletion attraction. In particular, the nature of solvent and of the polymer (with its concentration) may affect each of these forces and modify the final NP stability. The only robust means of getting good dispersion is to use solvents where the P2VP strongly adsorbs on the silica surface, such as MEK. The creation of a bound layer, whose thickness is on the order of R_g of the polymer, imposes strong steric repulsion between NPs and thus prevents particle agglomeration in PNCs. In the case of pyridine, since a bound layer is not created, NP dispersion represents a subtle balance among electrostatic repulsions between the NPs, polymer-induced attraction, and NP dynamics. These results strongly argue for the critical role played by the solvent in creating the initial NP dispersion state. Since NP–NP attractions are strong in the agglomerated state, it is apparent that the initial dispersion state cannot be easily changed through subsequent thermal annealing. Thus, the properties of many PNCs are determined by the solvent from which they are processed. Our work points out the critical role played by this often ignored variable, present in different fields of the polymer physics, e.g., polymer crystallization,³⁵ polymer crystals decorated NPs,³⁶ or self-assemblies of Janus NPs.³⁷

■ ASSOCIATED CONTENT

● Supporting Information

Details of static and dynamic light scattering; Figures S0–S6 and Tables S1–S3. This material is available free of charge via the Internet at <http://pubs.acs.org>.

■ AUTHOR INFORMATION

Corresponding Author

*E-mail: sk2794@columbia.edu (S.K.K.).

Present Address

N.J.: Sorbonne Universités, UPMC Université Paris 06, CNRS UMR 8234, PHENIX, F-75005, Paris, France.

Notes

The authors declare no competing financial interest.

■ ACKNOWLEDGMENTS

The authors thank the National Science Foundation (NSF DMR 1006514) for partial funding of this research.

■ REFERENCES

- Moniruzzaman, M.; Winey, K. I. Polymer nanocomposites containing carbon nanotubes. *Macromolecules* **2006**, *39* (16), 5194–5205.
- (a) Cassagnau, P. Melt rheology of organoclay and fumed silica nanocomposites. *Polymer* **2008**, *49* (9), 2183–2196. (b) Jancar, J.; Douglas, J. F.; Starr, F. W.; Kumar, S. K.; Cassagnau, P.; Lesser, A. J.; Sternstein, S. S.; Buehler, M. J. Current issues in research on structure-property relationships in polymer nanocomposites. *Polymer* **2010**, *51* (15), 3321–3343.
- Kumar, S. K.; Jouault, N.; Benicewicz, B.; Neely, T. Nanocomposites with polymer grafted nanoparticles. *Macromolecules* **2013**, *46* (9), 3199–3214.
- Mackay, M. E.; Tuteja, A.; Duxbury, P. M.; Hawker, C. J.; Van Horn, B.; Guan, Z. B.; Chen, G. H.; Krishnan, R. S. General strategies for nanoparticle dispersion. *Science* **2006**, *311* (5768), 1740–1743.
- Moll, J. F.; Kumar, S. K.; Snijkers, F.; Vlassopoulos, D.; Rungta, A.; Benicewicz, B.; Gomez, E.; Ilavsky, J.; Colby, R. H. Dispersing grafted nanoparticle assemblies into polymer melts through flow field. *ACS Macro Lett.* **2013**, *2*, 1051–1055.
- Vaia, R. A.; Maguire, J. F. Polymer nanocomposites with prescribed morphology: Going beyond nanoparticle-filled polymers. *Chem. Mater.* **2007**, *19* (11), 2736–2751.
- Jordan, J.; Jacob, K. I.; Tannenbaum, R.; Sharaf, M. A.; Jasiuk, I. Experimental trends in polymer nanocomposites - a review. *Mater. Sci. Eng., A* **2005**, *393* (1–2), 1–11.
- Bansal, A.; Yang, H. C.; Li, C. Z.; Cho, K. W.; Benicewicz, B. C.; Kumar, S. K.; Schadler, L. S. Quantitative equivalence between polymer nanocomposites and thin polymer films. *Nat. Mater.* **2005**, *4* (9), 693–698.
- (a) Jouault, N.; Vallat, P.; Dalmas, F.; Said, S.; Jestin, J.; Boue, F. Well-dispersed fractal aggregates as filler in polymer-silica nanocomposites: long-range effects in rheology. *Macromolecules* **2009**, *42* (6), 2031–2040. (b) Jouault, N.; Dalmas, F.; Boue, F.; Jestin, J. Multiscale characterization of filler dispersion and origins of mechanical reinforcement in model nanocomposites. *Polymer* **2012**, *53* (3), 761–775.
- (a) Sen, S.; Xie, Y.; Bansal, A.; Yang, H.; Cho, K.; Schadler, L. S.; Kumar, S. K. Equivalence between polymer nanocomposites and thin polymer films: Effect of processing conditions and molecular origins of observed behavior. *Eur. Phys. J.: Spec. Top.* **2007**, *141*, 161–165. (b) Hu, S. W.; Sheng, Y. J.; Tsao, H. K. Self-assembly of organophilic nanoparticles in a polymer matrix: Depletion interactions. *J. Phys. Chem. C* **2012**, *116* (2), 1789–1797.
- Janes, D. W.; Moll, J. F.; Harton, S. E.; Durning, C. J. Dispersion morphology of poly(methyl acrylate)/silica nanocomposites. *Macromolecules* **2011**, *44* (12), 4920–4927.
- Meth, J. S.; Zane, S. G.; Chi, C. Z.; Londono, J. D.; Wood, B. A.; Cotts, P.; Keating, M.; Guise, W.; Weigand, S. Development of filler structure in colloidal silica-polymer nanocomposites. *Macromolecules* **2011**, *44* (20), 8301–8313.
- (a) Kim, S. Y.; Hall, L. M.; Schweizer, K. S.; Zukoski, C. F. Long wavelength concentration fluctuations and cage scale ordering of nanoparticles in concentrated polymer solutions. *Macromolecules* **2010**, *43* (23), 10123–10131. (b) Kim, S. Y.; Schweizer, K. S.; Zukoski, C. F. Multiscale structure, interfacial cohesion, adsorbed layers, and thermodynamics in dense polymer-nanoparticle mixtures. *Phys. Rev. Lett.* **2011**, *107* (22), 225504. (c) Kim, S. Y.; Zukoski, C. F. Particle restabilization in silica/PEG/ethanol suspensions: How strongly do polymers need to adsorb to stabilize against aggregation? *Langmuir* **2011**, *27* (9), 5211–5221. (d) Kim, S. Y.; Zukoski, C. F. Role of

- polymer segment-particle surface interactions in controlling nanoparticle dispersions in concentrated polymer solutions. *Langmuir* **2011**, *27* (17), 10455–10463.
- (14) Jouault, N.; Moll, J. F.; Meng, D.; Windsor, K.; Ramcharan, S.; Kearney, C.; Kumar, S. K. Bound polymer layer in nanocomposites. *ACS Macro Lett.* **2013**, *2* (5), 371–374.
- (15) (a) van Zanten, J. H.; Wallace, W. E.; Wu, W.-l. Effect of strongly favorable substrate interactions on the thermal properties of ultrathin polymer films. *Phys. Rev. E* **1996**, *53* (3), R2053–R2056. (b) Holt, A. P.; Sangoro, J. R.; Wang, Y. Y.; Agapov, A. L.; Sokolov, A. P. Chain and segmental dynamics of poly(2-vinylpyridine) nanocomposites. *Macromolecules* **2013**, *46* (10), 4168–4173.
- (16) Chen, C. G.; Justice, R. S.; Schaefer, D. W.; Baur, J. W. Highly dispersed nanosilica-epoxy resins with enhanced mechanical properties. *Polymer* **2008**, *49* (17), 3805–3815.
- (17) Schartl, W. *Light Scattering from Polymer Solutions and Nanoparticle Dispersions*; Springer: Berlin, 2007.
- (18) Huggins, M. L. The viscosity of dilute solutions of long-chain molecules. IV. Dependence on concentration. *J. Am. Chem. Soc.* **1942**, *64*, 2716–2718.
- (19) Mori, S.; Barth, H. G. *Size Exclusion Chromatography*; Springer: Berlin, 1999.
- (20) Doane, T. L.; Chuang, C. H.; Hill, R. J.; Burda, C. Nanoparticle zeta-potentials. *Acc. Chem. Res.* **2012**, *45* (3), 317–326.
- (21) Percus, J. K.; Yevick, G. J. Analysis of classical statistical mechanics by means of collective coordinates. *Phys. Rev.* **1958**, *110* (1), 1–13.
- (22) (a) Hayter, J. B.; Penfold, J. An analytic structure factor for macroion solutions. *Mol. Phys.* **1981**, *42* (1), 109–118. (b) Hansen, J. P.; Hayter, J. B. A rescaled MSA structure factor for dilute charged colloidal dispersions. *Mol. Phys.* **1982**, *46* (3), 651–656.
- (23) Gogelein, C.; Tuinier, R. Phase behaviour of a dispersion of charge-stabilised colloidal spheres with added non-adsorbing interacting polymer chains. *Eur. Phys. J. E* **2008**, *27* (2), 171–184.
- (24) Hsu, M. F.; Dufresne, E. R.; Weitz, D. A. Charge stabilization in nonpolar solvents. *Langmuir* **2005**, *21* (11), 4881–4887.
- (25) Israelachvili, J. N. *Intermolecular and Surface Forces*; Academic Press: London, 1985.
- (26) Vincent, B.; Edwards, J.; Emmett, S.; Jones, A. Depletion flocculation in dispersions of sterically-stabilized particles (soft spheres). *Colloids Surf.* **1986**, *18* (2–4), 261–281.
- (27) Cohen Stuart, M. A.; Fleer, G. J.; Scheutjens, J. M. H. M. Displacement of polymers. II. Experiment, determination of segmental adsorption energy of poly(vinylpyrrolidone) on silica. *J. Colloid Interface Sci.* **1984**, *97*, 526–535.
- (28) (a) Hooper, J. B.; Schweizer, K. S. Contact aggregation, bridging, and steric stabilization in dense polymer-particle mixtures. *Macromolecules* **2005**, *38* (21), 8858–8869. (b) Hooper, J. B.; Schweizer, K. S. Theory of phase separation in polymer nanocomposites. *Macromolecules* **2006**, *39* (15), 5133–5142.
- (29) Harton, S. E.; Kumar, S. K.; Yang, H. C.; Koga, T.; Hicks, K.; Lee, E.; Mijovic, J.; Liu, M.; Vallery, R. S.; Gidley, D. W. Immobilized polymer layers on spherical nanoparticles. *Macromolecules* **2010**, *43* (7), 3415–3421.
- (30) Asakura, S.; Oosawa, F. On interaction between 2 bodies immersed in a solution of macromolecules. *J. Chem. Phys.* **1954**, *22* (7), 1255–1256.
- (31) Vrij, A. Polymers at interfaces and interactions in colloidal dispersions. *Pure Appl. Chem.* **1976**, *48* (4), 471–483.
- (32) Joanny, J. F.; Leibler, L.; Degennes, P. G. Effects of polymer-solutions on colloid stability. *J. Polym. Sci., Part B: Polym. Phys.* **1979**, *17* (6), 1073–1084.
- (33) Tuinier, R.; Rieger, J.; de Kruif, C. G. Depletion-induced phase separation in colloid-polymer mixtures. *Adv. Colloid Interface Sci.* **2003**, *103* (1), 1–31.
- (34) Scheutjens, J.; Fleer, G. J. Statistical-theory of the adsorption of interacting chain molecules. 1. Partition-function, segment density distribution, and adsorption-isotherms. *J. Phys. Chem.* **1979**, *83* (12), 1619–1635.
- (35) Somani, R. H.; Yang, L.; Zhu, L.; Hsiao, B. S. Flow-induced shish-kebab precursor structures in entangled polymer melts. *Polymer* **2005**, *46* (20), 8587–8623.
- (36) Li, C. Y. Polymer single crystal meets nanoparticles. *J. Polym. Sci., Part B: Polym. Phys.* **2009**, *47* (24), 2436–2440.
- (37) Jiang, S.; Chen, Q.; Tripathy, M.; Luijten, E.; Schweizer, K. S.; Granick, S. Janus particle synthesis and assembly. *Adv. Mater.* **2010**, *22* (10), 1060–1071.